

An Efficient Gradient-Sensitive Alternate Framework for VQE with Variable Ansatz

Ze-Tong Li^{1,3,4}, Fan-Xu Meng^{2,3,4}, Han Zeng^{2,3,4}, Zai-Chen Zhang^{2,3,4,5}, and Xu-Tao Yu^{1,3,4,5}

¹State Key Laboratory of Millimeter Waves, Southeast University, Nanjing 210096, China

²National Mobile Communications Research Laboratory, Southeast University, Nanjing 210096, China.

³Frontiers Science Center for Mobile Information Communication and Security, Southeast University, Nanjing 210096, China.

⁴Quantum Information Center, Southeast University, Nanjing 210096, China.

⁵Purple Mountain Lab, Nanjing 211111, China.

Variational quantum eigensolver (VQE), aiming at determining the ground state energy of a quantum system described by a Hamiltonian on noisy intermediate scale quantum (NISQ) devices, is among the most significant applications of variational quantum algorithms (VQAs). However, the accuracy and trainability of the current VQE algorithm are significantly influenced due to the *barren plateau* (BP), the non-negligible gate error and limited coherence time in NISQ devices. To tackle these issues, a gradient-sensitive alternate framework with variable ansatz is proposed in this paper to enhance the performance of the VQE. We first propose a theoretical framework for VA-VQE via alternately solving a multi-objective optimization problem and the original VQE, where the multi-objective optimization problem is defined with respect to cost function values and gradient magnitudes. Then, we propose a novel implementation method based on the double ϵ -greedy strategy with the candidate tree and modified multi-objective genetic algorithm. As a result, the local optima are avoided both in ansatz and parameter perspectives, and the stability of output ansatz is enhanced. The experimental results indicate that our framework shows considerably improvement of the error of the found solution by up to 87.9% compared with the hardware-efficient ansatz. Furthermore, compared with the full-randomized VA-VQE implementation, our framework is able to obtain the improvement of the error and the stability by up to 36.0% and 58.7%, respectively, with similar quantum costs.

1 Introduction

Quantum computing, a promising paradigm for solving many classically intractable problems [1, 2, 3, 4], is confronted with the era of noisy intermediate scale quantum (NISQ) [5]. NISQ devices, characterized as tiny quantities and short coherent time of qubits and low fidelity of quantum gates, seem difficult to efficiently apply the extraordinary quantum algorithms.

Fan-Xu Meng: Equal contribution to Ze-Tong Li

Xu-Tao Yu: yuxutao@seu.edu.cn

A hybrid quantum-classical scheme kindles the hope of extracting the quantum advantages from NISQ devices. In this scheme, the quantum computer maintains a parameterized quantum circuit (aka. ansatz), and the classical computer runs an optimizer to find the parameters that minimize the cost function of the ansatz. This novel scheme was first proposed as the variational quantum eigensolver (VQE) [6] to find the ground-state energy, and generalized for solving linear systems [7], simulating dynamics [8], decomposing matrix [9, 10], reducing the dimensionality of data [11], and solving problems in the data science domain [12, 13, 14]. In the following text, the term VQE is used to indicate all methods that adopt the aforementioned scheme.

The VQE has experimentally shown effectiveness in small-scale problems [15]. The elaborately engineered ansatzes [16] with fixed layer structure and adjustable cardinality of layers have impressively exhibited high expressibility, the ability to express the extensive range of quantum states. However, the performance of VQE with the ansatzes degrades significantly with the qubit number and circuit depth [17]. The phenomena of the degradation are generally exhibited as the non-ignorable absolute error between the converged cost function value and the exact minimum.

One reason for the degradation is that the VQE suffers from the so-called barren plateau [18] that the gradient magnitudes vanish exponentially with the system scale. Then, the severity of the BP phenomenon is linked to the number of entanglements [19, 20, 21, 22] and the expressibility [23]. Another reason is quantum hardware noise both in quantum gates and qubits. The influence of the noise accumulates with the number of quantum gates and the circuit depth [24] and causes the accuracy reduction of the observable estimation. This significantly impedes the convergence of the cost function since the value of the cost function and its gradient are inaccurate, which is known as noise-induced barren plateaus [24].

Recently, the variable ansatz strategy [17, 25, 26, 27, 28, 29, 30] has emerged as a promising technique to reserve the quantum advantage in large-scale situations. Unlike the structure fixed ansatz, the layer constraint is relaxed in variable ansatz, and gates can be added anywhere in the ansatz as required. As a result, both the size and the depth of the constructed ansatz can be effectively reduced, and thus better solutions can be found. Nevertheless, implementing the VQE with variable ansatz (VA-VQE) exists a significant space overhead for the ansatz layout optimization procedure, and consequently requires substantially more computing resources than that with the structure fixed ansatz.

To further improve efficiency, several techniques from intelligent algorithms have also been introduced. Several methods based on the complete training are proposed [25, 27, 28, 31]. In these methods, the performance estimation of an ansatz requires VQE training until the cost function converges to obtain the lowest cost function value of the ansatz. As a result, high precision of the optimal selection among sampled ansatzes is achieved but undesirably introduces tremendous cost function determinations which are time-consuming because each determination of cost function requires substantial quantum measurements. Therefore, the range of sampled ansatzes is narrow when the quantity of quantum measurements is limited. This may result in local optimum from the ansatz perspective.

Attempting to overcome this hurdle, several methods based on the highly shared parameter pool are proposed [17, 30]. These methods construct ansatzes layer-wisely and maintain parameter pools from which values of parameters are exploited to calculate the cost function value as the performance predictor. Introducing the weight-sharing policy [32], parameters are shared among layers with similar structures. Thus, the number of parameters in the parameter pool required to be trained is effectively reduced. These methods first train the parameter pools iteratively. In each iteration, several ansatzes are sampled

based on the sampling strategy. Then, the parameters corresponding to the ansatzes are updated in specified steps (especially one step) by an optimizer. After training the parameter pools, the optimal ansatz selection procedure is processed. Quantities of ansatzes are sampled and evaluated by the performance predictor. Finally, the ansatz with the best performance, generally the lowest cost function value, is selected as the optimal ansatz.

This kind of method gains the efficiency in finding optimal ansatz by avoiding complete training of ansatzes. However, since the parameters are highly shared and the training step of each ansatz is insufficient to converge, the current cost function values may not express the actual performances of the ansatzes, and hence the output suffers from high variance. This may result from two issues. The first is the training competitions that values of parameters in ‘good’ ansatzes with promising layouts may be disturbed by the training of ‘bad’ ansatzes incurred by the weight-sharing policy. The second issue is that the policy for ansatz layout optimization exploits the cost function value only as the benchmark to find the optimal ansatz structure. The mediocre ansatz whose cost function value is currently the lowest and cannot be further decreased may be selected as the optimum. Contrarily, the promising ansatzes may be discarded because of their temporarily high cost function values.

In this paper, addressing these issues, we propose a gradient-sensitive alternate framework (GSA) for VA-VQE. The GSA alternately optimizes the structure of the ansatz and corresponding parameters by emphasizing the gradient magnitudes. Contributions are listed below:

- We first propose a theoretical framework solving VA-VQE via alternately for solving a gradient magnitudes related multi-objective optimization problem and the original VQE, so that local optima can be avoided from the ansatz perspective and the stability is enhanced compared to other VA-VQE methods.
- To mitigate training competitions in training the parameter pool for the initialization of parameters, we first exploit the double ϵ -greedy strategy based on the candidate tree to differentiate ansatzes by their cost function values and the gradient magnitudes, so that local optima can be evaded from the parameter perspective.
- We further reduce the size of the search space of the ansatz via applying gate commutation rules and establishing a bijection between the search space and the practical implementations of ansatzes to boost the time efficiency of the optimal ansatz and parameter determination.
- We adopt relatively fair criteria for measuring the performance of VA-VQE so that the transverse comparison among methods of VA-VQE can be conducted. As a result, the GSA shows conspicuously better performance on average compared to the structure fixed HEA up to 87.9% improvement in terms of absolute error, and to the full-randomized VA-VQE method up to 36.0% and 58.7% improvement in terms of absolute error and stability (mean square error), respectively, with similar quantum costs (the number of calculations of the cost function).

This paper is structured as follows: In Sec. 2, we give a brief introduction to the basic knowledge. Then, the gradient-sensitive theoretical framework based on the alternate optimization is proposed in Sec. 3. The detail of the practical implementation of GSA is proposed in Sec. 4. Subsequently, we conduct numerical simulations with relatively fair criteria in Sec. 5 to show the advantages of our proposed method. Finally, we conclude this work in Sec. 6. Notice that the examples and pseudocodes of algorithms are summarized in Appendix A and F, respectively.

2 Background

2.1 Variational Quantum Eigensolver

In this work, we address the variational quantum eigensolver (VQE) tasks identified by sets of tuples $\mathbb{T} = \{(O_i, \rho_i, f_i)\}$ aiming at minimizing a cost function

$$C(\boldsymbol{\theta}) = \sum_i f_i(\text{Tr} [O_i U(\boldsymbol{\theta}) \rho_i U^\dagger(\boldsymbol{\theta})]), \quad (1)$$

where $\{\rho_i\}$ is the training set formed as n-qubit quantum states, $U(\boldsymbol{\theta})$ is a specified parameterized quantum circuit (aka. ansatz) with parameters $\boldsymbol{\theta}$, O_i are observables and f_i are bounded second-order differentiable functions that encode the problem with respect to the operand observable O_i and state ρ_i . Generally, while implementing the VQE, the quantum computer applies the ansatz $U(\boldsymbol{\theta})$ and processes the quantum measurements to determine expectations $\text{Tr} [O_i U(\boldsymbol{\theta}) \rho_i U^\dagger(\boldsymbol{\theta})], \forall i$. The classical computer computes the cost function value and runs an optimization algorithm to find the optimal parameters $\boldsymbol{\theta}^*$ that minimize the cost function. We provide an example finding the ground state energy of a quantum system described by a Hamiltonian in Eg. 1.

2.2 Quantum Gradient

In the optimization procedure of large-scale VQE, the gradient-based methods (e.g., gradient descent) are generally more preferred than gradient-free methods (e.g., Nelder-Mead) [33]. In the gradient-based methods, the gradient of the cost function with respect to the parameters is essentially estimated in each optimization iteration.

Without loss of generality, an ansatz can be mathematically defined by

$$U(\boldsymbol{\theta}) := \prod_{l=1}^{N_l} U_l(\theta_l) W_l, \quad (2)$$

where $U_l(\theta_l) = \exp(-i\theta_l V_l)$, V_l is a Hermitian operator, and W_l is a non-parametrized quantum gate. Then, the partial derivative of an expectation $E(\boldsymbol{\theta}) = \text{Tr}(OU(\boldsymbol{\theta})\rho U^\dagger(\boldsymbol{\theta}))$ with respect to the k th parameter θ_k is

$$\partial_k E(\boldsymbol{\theta}) \equiv \frac{\partial E(\boldsymbol{\theta})}{\partial \theta_k} = i \text{Tr} \left([V_k, U_L^\dagger O U_L] U_R \rho U_R^\dagger \right), \quad (3)$$

where we use the notations

$$U_R \equiv \prod_{l=1}^{k-1} U_l(\theta_l) W_l, \quad U_L \equiv \prod_{l=k}^{N_l} U_l(\theta_l) W_l. \quad (4)$$

In this paper, we apply the parameter-shift rule [33] for gradient estimating. We assume that all parameterized quantum gates are Pauli rotations. Therefore, the partial derivative of $E(\boldsymbol{\theta})$ with respect to θ_k is

$$\partial_k E(\boldsymbol{\theta}) = \frac{1}{2} \left[E(\boldsymbol{\theta} + \frac{\pi}{2} \mathbf{e}_k) - E(\boldsymbol{\theta} - \frac{\pi}{2} \mathbf{e}_k) \right], \quad (5)$$

where \mathbf{e}_k is a vector whose k th element is 1 and others are 0.

2.3 Gradient Descent

Gradient descent is literally a gradient-based optimizer that has been generally used in training VQE [7, 8, 11, 12]. The kernel process of the gradient descent can be mathematically represented as

$$\boldsymbol{\theta} \leftarrow \boldsymbol{\theta} - \alpha \nabla C(\boldsymbol{\theta}), \quad (6)$$

where α is the step size.

In this paper, we exploit a line search to estimate the step size α instead of a fixed one. In each optimization step, α satisfies the Wolfe conditions [34]

$$C(\boldsymbol{\theta} - \alpha \mathbf{g}) \leq C(\boldsymbol{\theta}) - c_1 \alpha \|\mathbf{g}\|_2^2, \quad (7)$$

$$\nabla C(\boldsymbol{\theta} - \alpha \mathbf{g})^T \mathbf{g} \geq c_2 \|\mathbf{g}\|_2^2, \quad (8)$$

where $\mathbf{g} = \nabla C(\boldsymbol{\theta})$ and $0 < c_1 < c_2 < 1$. To facilitate the α determination, given a reference step size α_0 , we gradually decrease α from α_0 by repeating $\alpha \leftarrow \rho \alpha$ until Eq. (7) establishes, where $\rho < 0$. In this paper, we empirically set $c_1 = 10^{-4}$ and $\rho = 0.618$.

2.4 Expressibility

In the absence of prior knowledge about the solution unitaries \mathbb{U}_s of a VQE task, the ability of ansatz to generate a wide range of unitaries \mathbb{U} to guarantee $\mathbb{U}_s \cap \mathbb{U} \neq \emptyset$ is required. The expressibility of an ansatz describes the degree to which it uniformly explores the unitary group $\mathcal{U}(2^n)$, and can be simply considered as the range of unitaries the ansatz can generate. By comparing the uniform distribution of unitaries obtained from \mathbb{U} to the Haar distribution of unitaries from \mathcal{U} , the expressibility of an ansatz can be defined by the superoperator [35, 36]:

$$\mathcal{A}_u^{(t)} := \int_{\mathcal{U}(2^n)} d\mu(V) V^{\otimes t} (\cdot) (V^\dagger)^{\otimes t} - \int_{\mathbb{U}} dU U^{\otimes t} (\cdot) (U^\dagger)^{\otimes t}, \quad (9)$$

where $d\mu(V)$ is the volume element of the Haar measure and dU is the volume element corresponding to the uniform distribution over \mathbb{U} . Here we are especially interested in the expressibility of the ansatz with respect to the input quantum state ρ and the observable O

$$\epsilon_{\mathbb{U}}^\rho := \left\| \mathcal{A}_{\mathbb{U}}^{(2)}(\rho^{\otimes 2}) \right\|_2, \quad \epsilon_{\mathbb{U}}^O := \left\| \mathcal{A}_{\mathbb{U}}^{(2)}(O^{\otimes 2}) \right\|_2. \quad (10)$$

Small values of $\epsilon_{\mathbb{U}}^\rho$ and $\epsilon_{\mathbb{U}}^O$ indicate the high expressibility of the ansatz.

2.5 Barren Plateau and Trainability

As one of the key challenges of VQE, the barren plateau phenomenon exhibited the exponential decrement of the gradient magnitudes with respect to the system size n [18] and was generalized that the ansatzes' expressibility [23] and the amount of entanglement [19, 20, 21, 22] play significant roles in leading to barren plateaus. We highlight the severity of the BP phenomenon with respect to n and the expressibility of the ansatz by the limited variance of gradient magnitudes

$$\text{Var}[\partial_k C(\boldsymbol{\theta})] \leq \frac{g(\rho, O, U)}{2^{2n} - 1} + f(\epsilon_{\mathbb{U}_L}^O, \epsilon_{\mathbb{U}_L}^\rho), \quad (11)$$

where $g(\rho, O, U)$ is the prefactor in $O(2^n)$,

$$f(x, t) = 4xy + \frac{2^{n+2} \left(x \|O\|_2^2 + y \|\rho\|_2^2 \right)}{2^{2n} - 1}, \quad (12)$$

and \mathbb{U}_L and \mathbb{U}_R are ensembles of U_L and U_R , respectively [23]. The first term on the right in Eq. (11) indicates the variance of 2-design ansatz and is in $O(1/2^n)$, and the second term is the expressibility-dependent correction. From the Chebyshev's inequality, the trainability of an ansatz can be described by

$$\Pr [|\partial_k C(\boldsymbol{\theta})| \geq \delta] \leq \frac{\text{Var}[\partial_k C(\boldsymbol{\theta})]}{\delta^2}, \quad \forall \delta > 0. \quad (13)$$

When the ansatz exhibits the BP phenomenon, the probability decreases exponentially with respect to n , which indicates that the precision to determine a cost-minimizing direction is exponentially large to n [28, 37, 38]. Notably, an ansatz with higher expressibility suffers lower trainability since it exhibits a more severe BP phenomenon.

Remarkably, there exists another kind of barren plateaus, the noise-induced barren plateaus [24], caused by the imperfect quantum hardware. The cost function value concentrates exponentially around its average as the influence of noise accumulates, since the noise models acting throughout the ansatz map the input state toward the fixed point of the noise model [24, 39].

This challenging phenomenon cannot simply be escaped by changing the optimizer [38]. While several attempts have been made to mitigate the severity of the barren plateau [40, 41, 42, 43, 44], it is widely accepted that the variable ansatz strategy is promising to address this issue via automatically balancing the expressibility, the influence of noise, and the trainability.

2.6 Hardware Constraints

Generally, only a limited number of gates are available on a practical quantum computer and the two-qubit gates are only allowed to be applied on a specific set of qubit pairs. These available gates are known as native gates of the quantum hardware. In this paper, we assume the native gates on an n -qubit quantum system to be R_y , R_z and CNOT mathematically represented as

$$R_y^q(\theta) = e^{-i\frac{\theta}{2}\sigma_y} = \begin{bmatrix} \cos \frac{\theta}{2} & -\sin \frac{\theta}{2} \\ \sin \frac{\theta}{2} & \cos \frac{\theta}{2} \end{bmatrix}, \quad (14)$$

$$R_z^q(\theta) = e^{-i\frac{\theta}{2}\sigma_z} = \begin{bmatrix} e^{-i\theta/2} & 0 \\ 0 & e^{i\theta/2} \end{bmatrix}, \quad (15)$$

$$\text{CNOT}^{q_a, q_b} = |0\rangle\langle 0|^{q_a} \otimes I^{q_b} + |1\rangle\langle 1|^{q_a} \otimes X^{q_b}, \quad (16)$$

where superscript q , q_a , and q_b indicate the qubits on which the quantum gates act, σ_y and σ_z are Pauli operators mathematically represented as

$$\sigma_y = \begin{bmatrix} 0 & -i \\ i & 0 \end{bmatrix}, \sigma_z = \begin{bmatrix} -1 & 0 \\ 0 & 1 \end{bmatrix}, \quad (17)$$

I is the identity quantum operation and X is the quantum *not* gate mathematically represented as

$$I = \begin{bmatrix} 1 & 0 \\ 0 & 1 \end{bmatrix}, X = \begin{bmatrix} 0 & 1 \\ 1 & 0 \end{bmatrix}. \quad (18)$$

Moreover, R_z^q and R_y^q can be applied for all $q \in \{1, 2, \dots, n\}$, while CNOT gates CNOT^{q_a, q_b} are unidirectionally available on adjacent qubit pairs, i.e., $q_b = (q_a + 1) \bmod n$. Note that the proposed framework can be easily adjusted for different native gate sets.

3 Theoretical Framework

In this section, we introduce the theoretical framework derived from the problem of VQE. Then, we equivalently transform the solving procedure into solving a series of multi-objective optimization problems related to gradient magnitudes.

Recall that a VQE task can be considered as minimizing a cost function, which is summarized in Prob. 1.

Problem 1 (VQE). *Given an ansatz $U(\boldsymbol{\theta})$ and a task \mathbb{T} , the problem of VQE is to find parameters that minimize the cost function $C(\boldsymbol{\theta})$, i.e.,*

$$\min_{\boldsymbol{\theta} \in \mathbb{D}^{N_p}} C(\boldsymbol{\theta}) = \sum_i f_i(\text{Tr} [O_i U(\boldsymbol{\theta}) \rho_i U^\dagger(\boldsymbol{\theta})]), \quad (19)$$

where $\mathbb{D} \subset \mathbb{R}$, N_p is the cardinality of trainable parameters $\boldsymbol{\theta}$.

While introducing the VA-VQE framework as summarized in Prob. 2, the structure of ansatz U is treated as a variable that needs to be optimized in the cost function

$$C(U, \boldsymbol{\theta}) = \sum_i f_i(\text{Tr} [O_i U(\boldsymbol{\theta}) \rho_i U^\dagger(\boldsymbol{\theta})]). \quad (20)$$

Problem 2 (VA-VQE). *Given a search space of ansatz \mathbb{S} and a task \mathbb{T} , the problem of VA-VQE is to find ansatzes and corresponding parameters that minimize the cost function $C(U, \boldsymbol{\theta})$, i.e.,*

$$\min_{U \in \mathbb{S}, \boldsymbol{\theta} \in \mathbb{D}^{N_p}} C(U, \boldsymbol{\theta}), \quad (21)$$

where $C(U, \boldsymbol{\theta})$ forms as Eq. (20), $\mathbb{D} \subset \mathbb{R}$, and N_p is the cardinality of trainable parameters $\boldsymbol{\theta}$.

Practically, the VA-VQE methods automatically construct ansatzes by quantum gates from a given gate set \mathbb{G} , i.e. $\mathbb{S} = \mathbb{G}^\infty$, and find ones with trained parameters that minimize the cost function. The search space of ansatz actually scales infinitely since the depth of ansatz circuits can be infinitely large. However, the trainability of the ansatz is substantially limited by the number of quantum gates because the expressibility and the impact of noise of the ansatz may increase with respect to the number of quantum gates, which aggravates the BP phenomenon. On the other hand, it is intractable to search for solutions with enormous (even infinite) search space of ansatz. Therefore, a fixed or gradually increased maximum number n_g of quantum gates is introduced as $\mathbb{S} = \mathbb{G}^{N_g}$, where N_g is sufficiently large that $\exists U \in \mathbb{G}^{N_g}$ such that $\mathbb{U} \cap \mathbb{U}_s \neq \emptyset$. Nevertheless, determining exact solutions requires solving combinatorial optimization in an exponentially large search space, which conceals the efficiency of VQE. Most methods [17, 26, 28, 30, 31] attempt to provide approximate solutions in polynomial complexity with respect to g . Although the gradient is generally estimated for the optimization of parameters, its magnitude is neglected to provide a guideline for the optimization of the structure of ansatz. Therefore, several undesirable phenomena listed below may occur:

1. The ansatz which exhibits severe barren plateau, and thus the gradient magnitude is highly close to 0, is selected to test the cost function value multiple times.
2. The trivial ansatz whose parameters are completely trained, i.e. the gradient magnitude is highly close to 0, is selected as the optimal ansatz since it temporarily cost less than potentially better ansatz with incompletely trained parameters, i.e. the gradient magnitude is significantly larger than 0.

These phenomena result in the local optimal of the VA-VQE from the ansatz perspective and instability of optimal ansatz and cost function value outputs.

Here we first introduce the gradient magnitude in solving the VA-VQE problem to explicitly supervise the severity of the BP phenomenon and the completeness of parameter training of ansatzes. We define a subproblem the gradient-related ansatz multi-objective optimization (GRAMO) in Prob. 3.

Problem 3 (GRAMO). *Given a search space of ansatzes \mathbb{S} , a task \mathbb{T} , and a set of parameters \mathbb{P} such that $\exists! \boldsymbol{\theta}_U \in \mathbb{P}, \forall U \in \mathbb{S}$, the problem of GRAMO is to find ansatzes that minimize the cost function $C(U, \boldsymbol{\theta}_U)$ and maximize the gradient magnitude of the cost function, i.e.,*

$$\min_{U \in \mathbb{S}} C(U, \boldsymbol{\theta}_U), \max_{U \in \mathbb{S}} \frac{\|\nabla C(U, \boldsymbol{\theta}_U)\|_2}{|\boldsymbol{\theta}_U|} \quad (22)$$

where $C(U, \boldsymbol{\theta}_U)$ forms as Eq. (20), $\nabla C(U, \boldsymbol{\theta}_U)$ is the gradient of $C(U, \boldsymbol{\theta}_U)$ with respect to $\boldsymbol{\theta}_U$, $\boldsymbol{\theta}_U \in \mathbb{P}$, and $|\boldsymbol{\theta}_U|$ is the cardinality of parameters in $\boldsymbol{\theta}_U$.

The (1-rank) solution of Prob. 3 is defined as the non-dominated set \mathbb{U}_n consisting of all U such that no $V \in \mathbb{S}$ simultaneously establishes inequalities

$$C(V, \boldsymbol{\theta}_V) < C(U, \boldsymbol{\theta}_U), \quad (23)$$

$$\frac{\|\nabla C(V, \boldsymbol{\theta}_V)\|_2}{|\boldsymbol{\theta}_V|} \geq \frac{\|\nabla C(U, \boldsymbol{\theta}_U)\|_2}{|\boldsymbol{\theta}_U|}. \quad (24)$$

As a result, structures of ansatzes with low cost function values or large gradient magnitudes, in other words, high absolute performance or high potentiality, are selected as solutions. Furthermore, the k -rank solution $\mathbb{U}_n(k)$ of the problem is defined by $\mathbb{U}_n(k) := \mathbb{U}_n(k-1) \cap \mathbb{U}'_n$, where \mathbb{U}'_n is the 1-rank solution of Prob. 3 with search space $\mathbb{S} \setminus \mathbb{U}_n^{k-1}$.

We solve the VA-VQE problem by alternately solving Prob. 1 and Prob. 3 as summarized in Alg. 1. When the gate set \mathbb{G} and the task \mathbb{T} are specified, for any initialization of \mathbb{P} , the VA-VQE can be solved iteratively. At each iteration, the non-dominated set \mathbb{U}_n is determined by solving Prob. 3 the GRAMO with \mathbb{P} . Then, the optimal parameters $\boldsymbol{\theta}_U \in \mathbb{P}$ are updated via solving Prob. 1 the VQE, $\forall U \in \mathbb{U}_n$. The alternate optimization procedure terminates until \mathbb{U}_n and \mathbb{P} are converged.

Theorem 1 (Convergence). *\mathbb{U}_n and \mathbb{P} in Alg. 1 converge such that $\forall (U \in \mathbb{U}_n, \boldsymbol{\theta}_U \in \mathbb{P})$ are solutions of Prob. 2 for all \mathbb{P}_0 satisfied that $\exists V \in \mathbb{S}$ such that*

$$\exists \boldsymbol{\theta}^*, C(V, \boldsymbol{\theta}^*) = \min_{U, \boldsymbol{\theta}} C(U, \boldsymbol{\theta}), \quad (25)$$

$$\forall \delta > 0, C(V, \boldsymbol{\theta}_V \in \mathbb{P}_0) \neq \max_{\boldsymbol{\theta} \in \Theta_{V, \delta}} C(V, \boldsymbol{\theta}), \quad (26)$$

where

$$\Theta_{V, \delta} = \{\boldsymbol{\theta} \mid \|\boldsymbol{\theta} - \boldsymbol{\theta}_V\|_2 < \delta\}. \quad (27)$$

Theorem 1 (c.f. Appendix C for the proof) indicates that solutions of VA-VQE can be determined by Alg. 1.

4 Solving VQE Tasks with Gradient Sensitive Variable Ansatz

In this section, the gradient-sensitive alternate framework (GSA) for VA-VQE is proposed in detail. As the VA-VQE problem described, GSA takes the gate set \mathbb{G} and the task \mathbb{T} as inputs. Based on the gate commutation rules, the search space of ansatz $\mathbb{S}(N_l)$ under the maximum number of layers N_l is reduced to boost the time efficiency of the optimal ansatz and parameters determination. Then, the quasi-optimal ansatz and corresponding trained parameters are output through three stages: *pool training*, *alternate training*, and *VQE retraining*. In the stage of *pool training*, a candidate tree T is constructed for double ϵ -greedy sampling and a parameter pool in which parameters are shared among ansatzes with similar structures is trained via exploiting the double ϵ -greedy strategy based on the candidate tree. As a result, a reasonable set of parameters \mathbb{P}_0 is generated as the initialization of parameters for the next stage. Based on the multi-objective genetic algorithm, the *alternate training* applies the framework described in Alg. 1 to solve the VA-VQE problem via alternately solving the GRAMO in Prob. 3 and the VQE in Prob. 1. Since the evolutionary algorithm is applied, the output ansatz is quasi-optimal and corresponding parameters may be incompletely trained. Therefore, the third stage *VQE retraining* is required to guarantee the completion of parameter training of the quasi-optimal ansatz. We summarize the GSA as Alg. 2.

Besides, there are several parameters needed to be defined before actually running (c.f. Tab. 4 in Appendix D for the summarizing). For the entire proposed framework, they are, respectively, the maximum number of layers N_l , the reference step size α_0 , the convergence threshold ξ , and the probabilities of greedy selection for the double ϵ -greedy strategy ϵ_1 and ϵ_2 . In the *pool training*, they are, respectively, the number of sampled ansatzes N_{s1} , the maximum number of ranks of ansatzes whose corresponding parameters are updated N_{r1} , the stable threshold for terminating the main process N_{t1} , the maximum iteration times in the prethermalization N_{i0} , and the maximum iteration times in the main process N_{i1} . In the *alternate training*, they are, respectively, the population size N_{s2} , the maximum number of ranks of ansatzes whose corresponding parameters are updated N_{r2} , the stable threshold N_{t2} , the optimization step in a generation N_o , and the maximum iteration times N_{i2} . In the *VQE retraining*, they include the maximum iteration times N_{i3} .

This section is organized as follows: In Sec. 4.1, we concretely propose the structure of the search space of ansatz for the GSA and conduct the size reduction to the search space based on the gate commutation rules. Subsequently, the *pool training*, *alternate training*, and *VQE retraining* stages are explained in Sec. 4.2, 4.3 and 4.4, respectively.

4.1 Search Space of Ansatz

Without violation of Eq. 2, we compose an ansatz in a layer-by-layer fashion as shown in Fig. 1. To be specific, each layer consists of a set of native disjoint single-qubit gates followed by a set of hardware-compliant disjoint CNOT gates. It can be easily derived that the number of all possible structures N_s of a layer is exponentially large with respect to the number of qubits n . We use the term state denoted by \mathbf{s}_j to indicate the j th structure is used. Then, an ansatz can be identified by a tuple of states

$$\left(\mathbf{s}^1, \mathbf{s}^2, \dots, \mathbf{s}^{N_l}\right),$$

where $\mathbf{s}^l \in S := \{\mathbf{s}_1, \mathbf{s}_2, \dots, \mathbf{s}_{N_s}\}$. As a result, the search space of ansatz $\mathbb{S}(N_l)$ can be specifically represented by a tree with N_l+1 layers (from layer 0 to N_l). A node at the layer $l > 0$ in the tree is uniquely identified by its parent node and the state, i.e., $\mathbf{v}^l := (\mathbf{v}^{l-1}, \mathbf{s}^l)$,

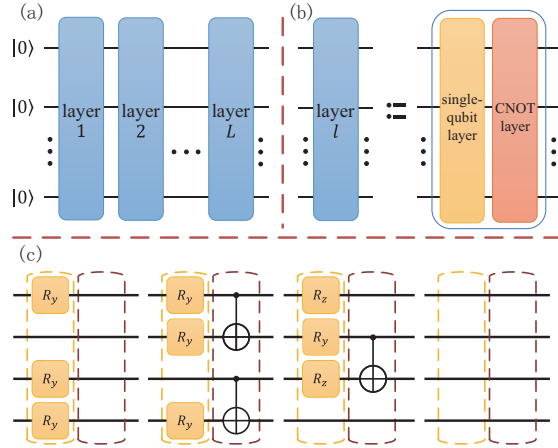


Figure 1: The layer-by-layer ansatz (a) with each layer being decomposed into two sublayers, i.e., (b) a single-qubit gate layer and a CNOT layer; and (c) four exemplary constructions of layers.

and linked to its child nodes. In layer 0, the root node of the tree is defined with no parent node and the state \mathbf{s}^0 in which no layer information is stored. Furthermore, we call the nodes in layer N_l linked to no child nodes the leaf nodes. Finally, a path from the root node to a leaf node $(\mathbf{v}^0, \mathbf{v}^1, \dots, \mathbf{v}^{N_l})$ represents an ansatz $(\mathbf{s}^1, \mathbf{s}^2, \dots, \mathbf{s}^{N_l})$.

The unrefined $\mathbb{S}(N_l)$ is intuitively a full N_s -ary tree with $(N_s)^{N_l}$ leaf nodes. However, this simple-minded construction can not establish the bijection between practical implementations of ansatzes and paths (c.f. Eg. 2). Moreover, gates in distinct layers may be deletable or mergeable (c.f. Eg. 3). To further eliminate the redundant ansatzes and improve the efficiency, the paths violating the following cross-layer constraints based on gate commutation rules will be pruned.

Constraints: For node $\mathbf{v}^l := (\mathbf{v}^{l-1}, \mathbf{s}^l)$ in the path $(\mathbf{v}^0, \mathbf{v}^1, \dots, \mathbf{v}^l)$:

1. $R_z^q, \text{CNOT}^{q,q'} \notin \mathbf{s}^l$, if R_y^q and $\text{CNOT}^{q'',q} \notin \mathbf{s}^k$, $\forall q$ with $|0\rangle$ initialization, q' and q'' , $l > k > 0$;
2. $\text{CNOT}^{q_1,q_2} \notin \mathbf{s}^l$, if $\exists \text{CNOT}^{q_1,q_2} \in \mathbf{s}^k$ such that $R_y^{q_1}, R_y^{q_2}, R_z^{q_2}, \text{CNOT}^{q',q_1}, \text{CNOT}^{q_2,q'}$, and $\text{CNOT}^{q',q_2} \notin \mathbf{s}^m$, $\forall q, q', k < m < l < 0$;
3. $R_z^q \notin \mathbf{s}^l$, if R_y^q and $\text{CNOT}^{q',q} \notin \mathbf{s}^{l-1}$, $\forall q, q', l > 0$;
4. $R_y^q \notin \mathbf{s}^l$, if $R_z^q, \text{CNOT}^{q,q'}$, and $\text{CNOT}^{q',q} \notin \mathbf{s}^{l-1}$, $\forall q, q', l > 1$.
5. \mathbf{s}^l is empty if \mathbf{s}^{l-1} is empty, $l > 1$.

The first constraint follows the fact that R_z^q and $\text{CNOT}^{q,q'}$ preserve the state of the quantum system when the quantum state of q is $|0\rangle$. The second constraint avoids two consecutive CNOT gates with identical control and target qubits. As a result, the first two constraints eliminate deletable combinations of quantum gates. The mergeable combinations are extinguished by constraints 3 and 4 by prohibiting consecutive R_z and R_y , respectively. Finally, the bijection between practical implementations of ansatzes and paths is established by the conjunction of constraints 3 to 5. Consequently, the size of the search space $|\mathbb{S}(N_l)|$ is significantly reduced. We provide an example Eg. 4 to demonstrate the efficiency obtained from our constraints.

4.2 Pool training

In this subsection, the *pool training* stage is presented in detail. Based on the weight-sharing policy, the number of parameters required to be trained is reduced to $\mathcal{O}(N_l)$. Moreover, the double ϵ -greedy strategy is exploited accompanied by a candidate tree to mitigate the training competitions among ansatzes. We treat the *pool training* as a one-shot training program. At each iteration, several ansatzes are randomly sampled and estimated. According to the estimated performance, several temporarily outstanding ansatzes are selected to update parameters in specified steps (typically one step) via a gradient-based optimizer.

Recall that solving VQ-VQE in the framework as described in Alg. 1 requires the initialization of \mathbb{P}_0 in which each structure of ansatz links to an independent set of parameters. Intuitively, that parameters $\boldsymbol{\theta}_U \in \mathbb{P}_0$ substantially reflect the actual performance of ansatz U , i.e., $\boldsymbol{\theta}_U \approx \arg \min_{\boldsymbol{\theta}} C(U, \boldsymbol{\theta})$, facilitates the optimal ansatz determination. Therefore, we conduct a pre-training of parameters before the alternate optimization solving VA-VQE instead of random initialization. Unfortunately, the size of \mathbb{P}_0 is exponentially large with respect to n and N_l resulting from the exponentially large $\mathbb{S}(N_l)$. It is impractical to adequately train \mathbb{P}_0 efficiently.

Instead, we construct a parameter pool with linear size with respect to N_l via applying the weight-sharing policy and train the pool to eventually derive \mathbb{P}_0 . The parameter pool can be matrix-like defined as

$$P := \begin{bmatrix} \boldsymbol{\theta}_{\mathbf{s}_1,1} & \boldsymbol{\theta}_{\mathbf{s}_1,2} & \cdots & \boldsymbol{\theta}_{\mathbf{s}_1,N_l} \\ \boldsymbol{\theta}_{\mathbf{s}_2,1} & \boldsymbol{\theta}_{\mathbf{s}_2,2} & \cdots & \boldsymbol{\theta}_{\mathbf{s}_2,N_l} \\ \vdots & \vdots & \ddots & \vdots \\ \boldsymbol{\theta}_{\mathbf{s}_{N_s},1} & \boldsymbol{\theta}_{\mathbf{s}_{N_s},2} & \cdots & \boldsymbol{\theta}_{\mathbf{s}_{N_s},N_l} \end{bmatrix}, \quad (28)$$

where $\boldsymbol{\theta}_{k,l}$ represents the parameters at the l th layer corresponding to the state \mathbf{s}_k . Then, parameters of an ansatz $(\mathbf{v}^0, \mathbf{v}^1, \dots, \mathbf{v}^{N_l})$ is

$$\boldsymbol{\theta} := \boldsymbol{\theta}_{\mathbf{s}^1,1} \oplus \boldsymbol{\theta}_{\mathbf{s}^2,2} \oplus \dots \oplus \boldsymbol{\theta}_{\mathbf{s}^{N_l},N_l}, \quad (29)$$

where \oplus indicates the direct sum such that

$$\begin{bmatrix} a_1 \\ a_2 \\ \vdots \\ a_N \end{bmatrix} \oplus \begin{bmatrix} b_1 \\ b_2 \\ \vdots \\ b_N \end{bmatrix} = \begin{bmatrix} a_1 \\ \vdots \\ a_N \\ b_1 \\ \vdots \\ b_N \end{bmatrix}.$$

It can be simply derived that parameters in identical layers and states are shared among ansatzes, which is the direct effect of applying the weight-sharing policy. Then, the number of trainable parameters is in $\mathcal{O}(N_s N_l)$, which is linear with respect to N_l . The exponentially reduction significantly boosts the efficiency of parameter training. However, the training competitions are therefore introduced.

Inspired by the ϵ -greedy strategy from traditional machine learning [45], we propose the double ϵ -greedy strategy based on the candidate tree to mitigate the training competitions. Remarkably, our proposed method not only differentiates ‘good’ and ‘bad’ ansatzes but also ansatzes among the two categories.

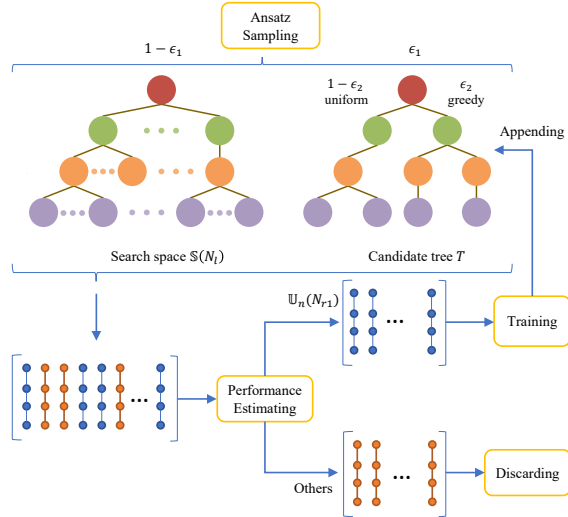


Figure 2: Single iteration of *pool training* with $N_l = 3$.

Recall that the search space $\mathbb{S}(N_l)$ can be represented by a tree. It is intuitive that constructing a tree to save potentially ‘good’ ansatzes and discarding potentially ‘bad’ ansatzes are reasonable for the differentiation. The tree spanned by paths representing potentially ‘good’ ansatzes is named the candidate tree. Each node \mathbf{v} in the tree maintains a leaf count $c_l(\mathbf{v})$ to indicate the number of leaf nodes below \mathbf{v} and a training count $c_t(\mathbf{v})$ to record the total times of training of the node. At each path sampling procedure, the GSA samples a path from the candidate tree with the probability ϵ_1 and the $\mathbb{S}(N_l)$ uniformly with the probability $1 - \epsilon_1$. While sampling from the candidate tree, nodes are successively sampled from the root to a leaf. Since only potentially ‘good’ ansatzes are appended to the candidate tree and recorded the training count of nodes via the one-shot training scheme, nodes in the candidate tree with a large training count may intuitively have more probability to construct potentially ‘good’ ansatzes. Let the last selected node be \mathbf{v}^{l-1} , $1 \leq l \leq N_l$, linked to child nodes $\mathbf{v}_1^l, \mathbf{v}_2^l, \dots, \mathbf{v}_{N_v}^l$. Then, the next node is sampled as \mathbf{v}_k^l with the probability

$$\Pr(\mathbf{v}_k^l; \eta) = \frac{c_l(\mathbf{v}_k^l) + \eta c_t(\mathbf{v}_k^l)}{\sum_{i=1}^{N_v} c_l(\mathbf{v}_i^l) + \eta c_t(\mathbf{v}_i^l)}, \quad (30)$$

where $\eta = 1$ with the probability ϵ_2 representing the greedy sampling and $\eta = 0$ with the probability $1 - \epsilon_2$ representing the uniform sampling. The ansatz sampling procedure is summarized as Alg. 3.

As depicted in Fig. 2, at each main process iteration of the *pool training*, the GSA samples N_{s1} paths exploiting the double ϵ -greedy strategy. Then, the cost function values and gradients of sampled ansatzes are estimated with corresponding parameters from the parameter pool. Subsequently, the N_{r1} -rank solution $\mathbb{U}_n(N_{r1})$ of Prob. 3 is determined among the sampled ansatzes. For each ansatz $U \in \mathbb{U}_n(N_{r1})$, corresponding parameters in the parameter pool are updated in one step via gradient descent optimizer. The main process terminates at iteration N_{i1} or when $c_l(\mathbf{v}^0)$ is stable that the value has been preserved for N_{t1} iterations which means there is no new path appended on the tree. As a result, the main process of the *pool training* is summarized as Alg. 4.

For the stability of *pool training*, we provide a prethermalization before the main process. Given an N_{i0} , at iteration i , the GSA processes as the main process iteration with

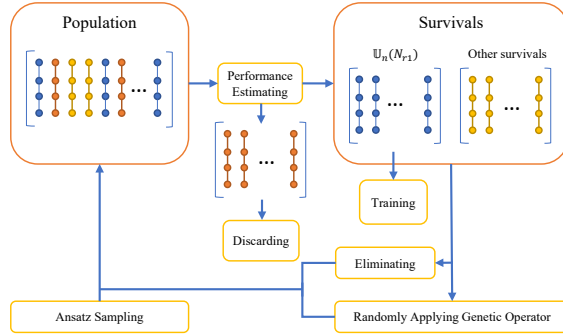


Figure 3: Single generation of *alternate training*.

$\epsilon'_1 = (i - 1)\epsilon_1/N_{i0}$ instead of ϵ_1 . The prethermalization of *pool training* is summarized as Alg. 5.

Finally, the *pool training* can be described by Alg. 6. After the initialization of P and T , the prethermalization and the main process are conducted to train P as well as T . Subsequently, the set of parameters \mathbb{P}_0 can be constructed by expanding P that θ_U is generated by Eq. (28) for any ansatz $U \in \mathbb{S}(N_l)$. The \mathbb{P}_0 and T are output for the next stage.

4.3 Alternate training

Recall that the VA-VQE can be solved via alternately solving Prob. 3 and Prob. 1. We exploit the multi-objective genetic algorithm with novel modification. The set of parameters \mathbb{P} is initialized as \mathbb{P}_0 . The individuals in the first generation are sampled independently via the double ϵ -greedy strategy as described in Sec. 4.2 to compose the initial population.

As shown in Fig. 3, at each generation (iteration), ansatzes in $\mathbb{U}_n(N_{r2})$ from solving Prob. 3 with respect to the population are trained to update \mathbb{P} in N_o steps via gradient descent optimizer. Note that the number of ansatzes in $\mathbb{U}_n(N_{r2})$ should be less than $N_{s2}/2$. Similar to the traditional genetic algorithm NGSA-II, $N_{s2}/2$ ansatzes are survived. Specifically, the GSA finds an N'_r such that

$$|\mathbb{U}_n(N'_r)| < N_{s2}/2 \leq |\mathbb{U}_n(N'_r + 1)|.$$

Then, ansatzes are sequentially inserted to survivals in increasing order of the cost function value from $\mathbb{U}_n(N'_r + 1) \setminus \mathbb{U}_n(N'_r)$. Subsequently, new ansatzes are generated by applying asexual genetic operators on survivals to fill the population. We leave the description of asexual genetic operators in Appendix E. Besides, we introduce the explicit elimination to the near-completely trained survivals U satisfying $\alpha \frac{\|\nabla C(U, \theta_U)\|_2}{|\theta_U|} < \xi$, where α is the step size. The eliminated ansatz is recorded if it has the temporarily lowest cost function value and is erased if there exists an ansatz with a lower cost function value. Notice that the elimination is conducted after the application of genetic operators. Therefore, the sampling based on the double ϵ -greedy is required to refill the population.

The *alternate training* terminates at the generation N_{i2} or when the record eliminated ansatz is preserved for N_{t2} generations. As a result, the ansatz U^* with the temporarily lowest cost function value is output as the quasi-optimal ansatz. Meanwhile, the corresponding parameters θ_{U^*} are output for the next stage as the parameter initialization. We summarize the *alternate training* in Alg. 7.

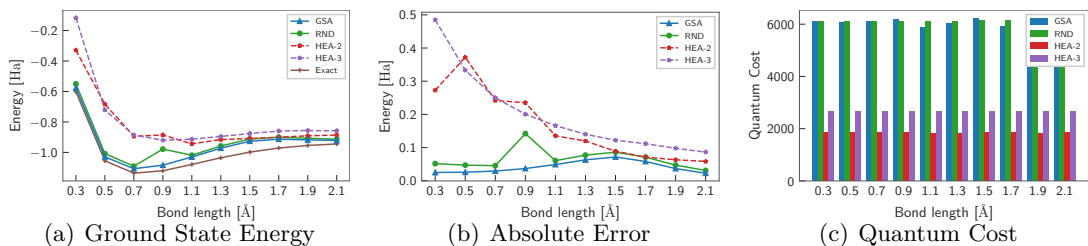


Figure 4: The average result of determining ground state energy of H₂ in various bond lengths among 100 running times.

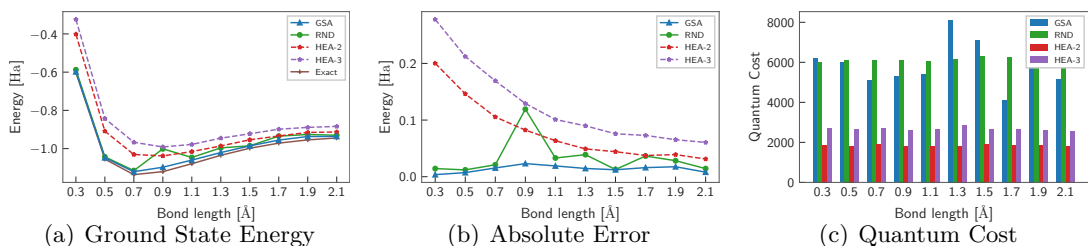


Figure 5: The best result of determining ground state energy of H₂ in various bond lengths among 100 running times.

4.4 VQE retraining

The final stage of *VQE retraining* inherits the quasi-optimal ansatz U^* and corresponding parameters θ_{U^*} output from the *alternate training* and provides a guarantee of the sufficiency of the parameter training of θ_{U^*} . As traditional VQE training does, this stage simply trains the parameters of θ_{U^*} with the initialization θ_{U^*} until the cost function value converges or the iteration count reaches N_{i3} . We summarize this stage as Alg. 8 for completeness.

5 Numerical Simulations

In this section, we conduct numerical simulations on VQE tasks for finding ground state energies of H₂ and H₄ molecules to show the improvement of the proposed framework. Moreover, to demonstrate the flexibility, we implement a modified version of the proposed framework for meta-VQE [46] learning energy profiles of parameterized Hamiltonians.

5.1 Finding ground state energies

To showcase the improvement of the proposed framework, we compare it with structure fixed hardware efficient ansatz (HEA) [16] and a fully randomized (RND) baseline algorithm. To make a fair comparison, we use Python with the *PennyLane* package [47] to implement both our and the two compared methods. The technical details for algorithms to be compared are elaborated as follows:

- **HEA.** HEA utilizes a fixed layer pattern to construct the whole circuit. The layer construction used in this implementation is depicted in Appendix B. Note that this kind of ansatzes is also widely used in other implementations, e.g., [10, 11];

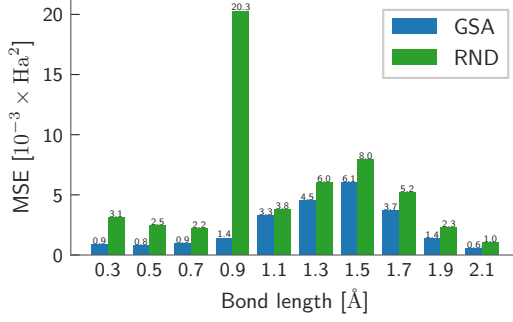


Figure 6: Mean square error among 100 running times.

- **RND.** We sample N_{Rs} circuits with N_l layers and unique random parameters, then process the VQE retraining and output the circuit with the minimum cost function value.

We assume that depolarization dominates the quantum error in the quantum hardware. Then, the noise operator (depolarizing channel) is

$$\Phi(p, \sigma) = \sum_{i=0}^3 K_i(p) \sigma K_i^\dagger(p),$$

$$K_0 = \sqrt{1-p} \begin{bmatrix} 1 & 0 \\ 0 & 1 \end{bmatrix}, K_1 = \sqrt{\frac{p}{3}} \begin{bmatrix} 0 & 1 \\ 1 & 0 \end{bmatrix}, K_2 = \sqrt{\frac{p}{3}} \begin{bmatrix} 0 & -i \\ i & 0 \end{bmatrix}, K_3 = \sqrt{\frac{p}{3}} \begin{bmatrix} 1 & 0 \\ 0 & -1 \end{bmatrix},$$

where $p \in [0, 1]$ is the depolarization probability and σ is a density matrix of a single qubit [47]. In our configuration, a depolarizing channel with depolarization probability $p = 0.001$ is applied after a single-qubit gate. We simultaneously apply two depolarizing channels with depolarization probability $p = 0.01$ after a CNOT, i.e., apply one on the control qubit, and one on the target qubit.

The criteria used for all methods are absolute error between the obtained and exact optimal cost function values, and the invoking times for the calculation of the cost function (termed *quantum cost* henceforth), respectively. For VA-VQE, we analyze the distribution of performances of output ansatzes and calculate the mean square error (MSE) mathematically represented by

$$MSE = \frac{1}{M} \sum_{i=1}^M (\hat{C}_i^* - C_{exact}^*)^2 \quad (31)$$

to indicate the stability to obtain the quasi-optimal cost function values, where M is the total running time, \hat{C}^* is the output quasi-optimal cost function value and C_{exact}^* is the exact optimal cost function value.

We first conduct numerical simulations on determining the ground state energies of Hamiltonians of H_2 in various bond lengths. The quantum device is assumed to have 4 qubits with ring connectives and depolarization error being imposed by the classical simulator. For the proposed framework, we empirical set $N_l = 3$, $\alpha_0 = 5$, $\xi = 0.003$, $\epsilon_1 = \epsilon_2 = 0.8$, $N_{s1} = N_{s2} = 16$, $N_{r1} = 1$, $N_{r2} = 2$, $N_{i0} = N_{i1} = 2$, $N_{i2} = 100$, $N_{i3} = 10$, $N_{t1} = 1$, $N_{t2} = 4$, and $N_o = 5$; for HEA, we exploit 2-layer HEA as HEA-2 and 3-layer HEA as HEA-3; for RND, we set $N_l = 3$ and $N_{Rs} = 6000$ such that the quantum costs of GSA and RND are approximately equal.

For each bond length, we conduct the GSA and comparison methods 100 times, respectively. The results on average are shown in Fig. 4. It can be found that our algorithm

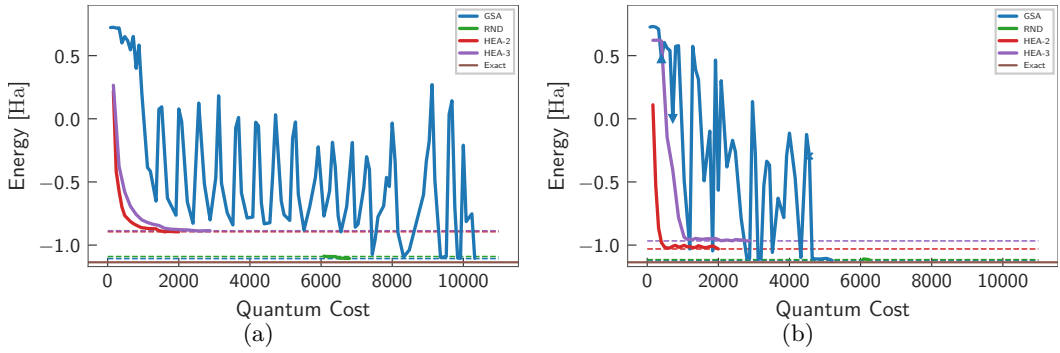


Figure 7: Detail of cost function values with respect to quantum cost in solving the ground state energy of H_2 in bond length 0.7\AA among 100 running times. (a) The average cost function values with respect to quantum cost. (b) The cost function values among 100 running times with respect to quantum cost in the running time which output the ansatz with the lowest cost function value among 100 running times. The \blacktriangle , \blacktriangledown , and \times represent the termination of *pool training*'s prethermalization, *pool training*'s main process, and *alternate training*, respectively.

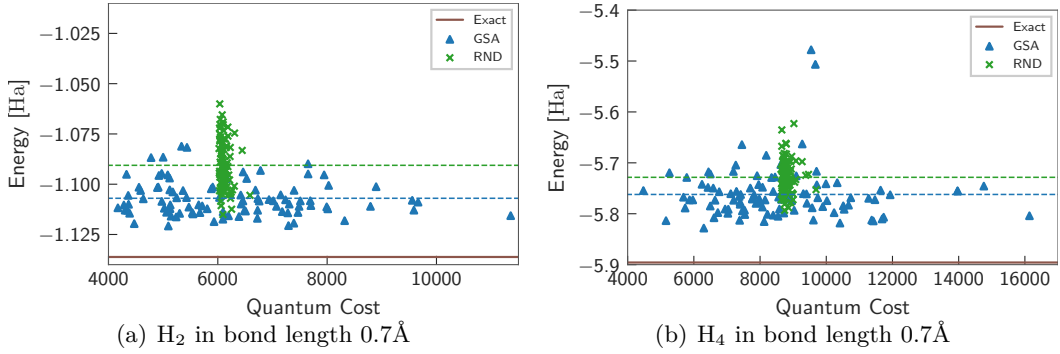


Figure 8: Output quasi-optimal cost function values with respect to the quantum cost of 100 running times in solving the ground state energy. Dashed lines present cost function values on average.

can determine ground state energy with consistently lower absolute error on average than the compared algorithms in terms of the absolute error in various bond lengths, and with lower quantum cost compared to RND. This conclusion holds while considering the ansatzes with the lowest cost function values among the 100 running times as depicted in Fig. 5. Moreover, GSA exhibits outstanding stability as shown in Fig. 6. Remarkably, VA-VQE methods performs better in terms of absolute error at a cost of quantum cost than HEA in most bond lengths.

For bond length 0.7\AA , we also record the quantum cost and absolute error for each running time in Fig. 7 and Fig. 8(a) when the algorithm converges to the final output result. It can be concluded that our algorithm can obtain the best solution on average with a rather small quantum cost (about 6107.49) which is conspicuously better than HEA (up to 87.9% improvement in terms of error) and RND (up to 36.0% and 58.7% improvement in terms of error and stability, respectively). Remarkably, GSA can asymptotically reach the best ansatz among the training, which means that a temporarily quasi-optimal ansatz can be output at any generation of *alternate training*. However, our framework shows large variance of the quantum cost. This may result from the termination conditions of the three stages. It can be concluded that the termination conditions prevent the redundant iterations which can not significantly benefit the training, and thus the performance of our

framework may not be sensitive to hyperparameters N_{i0} , N_{i1} , N_{i2} , and N_{i3} when they are sufficiently large.

Table 1: The result of determining the ground state energy of H_4 in bond length 0.7\AA . Data outside and inside brackets represent the average and the best values among 100 running times, respectively.

| | GSA | RND | HEA-2 | HEA-3 |
|---------------------|----------------|----------------|----------------|----------------|
| energy [Ha] | -5.762(-5.828) | -5.728(-5.793) | -5.350(-5.487) | -5.230(-5.439) |
| absolute error [Ha] | 0.134(0.068) | 0.167(0.103) | 0.546(0.408) | 0.666(0.457) |
| error improvement | - | 20.1%(34.1%) | 75.5%(83.4%) | 79.9%(85.2%) |
| quantum cost | 8579(6301) | 8811(8741) | 2665(2695) | 3865(3887) |
| stability | 0.020 | 0.029 | - | - |

We also conduct 6-qubit simulations for H_4 in bond length 0.7\AA . Configurations of GSA and HEA are set as them for H_2 . As for RND, we set $N_{Rs} = 8600$. Results of the simulations are shown in Tab. 1 and Fig. 8(b). Remarkably, the proposed method still shows significant improvements in terms of absolute error by up to 75.5% on average compared to HEA and both the absolute error and stability by up to 20.1% and 29.5%, respectively, compared to RND.

5.2 Learning energy profiles

To showcase the flexibility, we implement a modified version of the proposed framework for Meta-VQE [46]. Let the parameterized Hamiltonian be $H(\Delta)$. Then, sample M available values of Δ denoted by $\Delta_1, \Delta_2, \dots, \Delta_M$ as training bonds. Hence, the cost function for training Meta-VQE is defined by

$$C_{\text{Meta}}(\boldsymbol{\theta}) = \sum_{i=1}^M \text{Tr} \left[H(\Delta_i) U(\mathbf{f}(\Delta_i; \boldsymbol{\theta})) \rho_i U^\dagger(\mathbf{f}(\Delta_i; \boldsymbol{\theta})) \right], \quad (32)$$

where $\mathbf{f}(\Delta_i; \cdot)$ represents the encoding function of the parameter of the Hamiltonian with respect to operand trainable parameters. After parameter training, the landscape of

$$V_{\text{Meta}}(\Delta) = \text{Tr} \left[H(\Delta) U(\mathbf{f}(\Delta; \boldsymbol{\theta})) \rho_i U^\dagger(\mathbf{f}(\Delta; \boldsymbol{\theta})) \right] \quad (33)$$

exhibits the energy profile of the parameterized Hamiltonian.

We implement the Meta-VQE adapted GSA by simply identifying each state \mathbf{s} by both the structure and the encoding function of each single-qubit gate in the structure to enable the auto-decision of the encoding methods. Here we provide 3 encoding functions for parameters of single-qubit gates. They are, respectively,

$$f_1(\Delta; \theta) = \theta, \quad (34)$$

$$f_2(\Delta; \theta, \gamma) = \theta\Delta + \gamma, \quad (35)$$

$$f_3(\Delta; \theta, \gamma) = \theta e^\Delta + \gamma. \quad (36)$$

We compare our framework with the HEA implementation. Each HEA consists of N_{le} encoding layers and N_{lp} processing layers and is denoted by HEA- N_{le} - N_{lp} . Specifically, f_2 and f_1 are applied on each single-qubit gate in encoding layers and processing layers, respectively.

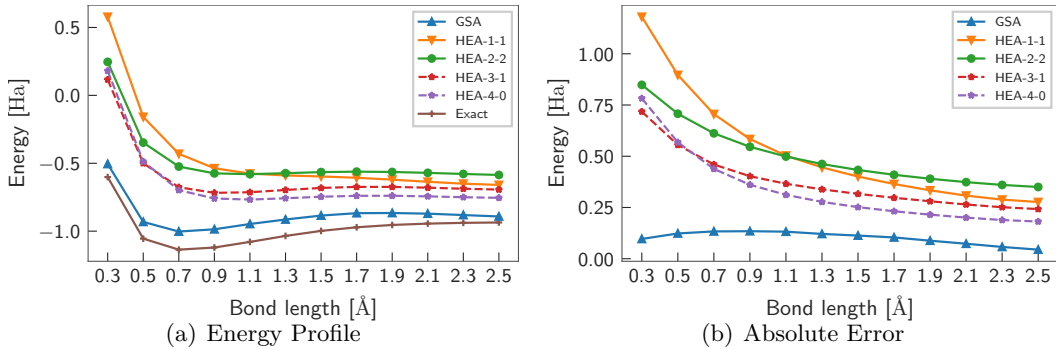


Figure 9: The result of determining the energy profile of H₂.

Table 2: The variance of absolute error and corresponding improvement.

| | GSA | HEA-1-1 | HEA-2-2 | HEA-3-1 | HEA-4-0 |
|-------------|-------|---------|---------|---------|---------|
| variance | 0.001 | 0.078 | 0.024 | 0.020 | 0.033 |
| improvement | - | 98.8% | 96.1% | 95.4% | 97.2% |

Simulations are conducted for H₂, where Δ in $H(\Delta)$ represents the bond length. Training bonds are set as 0.5, 0.9, 1.3, 1.7, 2.1, 2.5 and 2.9. We set $N_l = 4$ and other configurations as that for the VQE task of H₂. Results are shown in Fig. 9 and Tab. 2. It can be concluded that our framework learns the energy profile with the conspicuously lower variance of absolute error, which indicates more information on chemical properties.

6 Conclusion

In this paper, addressing the issues in mitigating the BP phenomenon in VQE, we propose a gradient-sensitive alternate framework for VQE with the variable ansatz strategy. We propose a theoretical framework that highlights the magnitude of gradient and exploits the alternate optimization scheme so that the local optimum can be avoided from the ansatz perspective. It can be theoretically proved that the result of the proposed theoretical framework is a subset of the results of the original VA-VQE.

Then, based on the theoretical framework, a novel implementation named GSA is proposed with three stages. We reduce the size of the search space of the ansatz via applying gate commutation rules and establishing a bijection between the search space and the practical implementations of ansatzes to boost the time efficiency of the optimal ansatz and parameter determination. Exploiting the double ϵ -greedy strategy based on the candidate tree, an initialization of parameters is determined, so that the training competitions are mitigated and the local optimal can be evaded from the parameter perspective. Based on the initialization of parameters, the GSA follows the framework with an elaborately modified genetic algorithm to find and train a quasi-optimal ansatz.

Finally, we conduct numerical simulations on quantum chemistry to find the ground state energy of a quantum system. We adopt relatively fair criteria for measuring the performance of VA-VQE so that the transverse comparison among methods of VA-VQE can be clearly conducted. As a result, the GSA shows conspicuously better performance on average compared to the structure fixed HEA up to 87.9% improvement in terms of absolute error. Furthermore, compared to the full-randomized RND, our framework obtains up to

36.0% and 58.7% improvement in terms of error and stability, respectively, with similar quantum costs. Moreover, we implement a modified version of our proposed framework for meta-VQE learning the energy profile of parameterized Hamiltonians to show the flexibility.

Although the proposed method obtained better results, further research is required to be conducted. For example, GSA requires a large number of hyperparameters to be adjusted such as N_l . Research on automatic hyperparameter adjustment may be meaningful for the VA-VQE.

Acknowledgements

This work was supported by the National Science Foundation of China (No. 61871111 and No. 61960206005) and the Fundamental Research Funds for the Central Universities (No. 2242022k30006 and No. 2242022k30001).

References

- [1] Lov K Grover. “Quantum computers can search arbitrarily large databases by a single query”. *Physical review letters* **79**, 4709 (1997).
- [2] Peter W Shor. “Polynomial-time algorithms for prime factorization and discrete logarithms on a quantum computer”. In *SIAM Review*. Volume 41, pages 303–332. SIAM (1999).
- [3] Aram W. Harrow, Avinatan Hassidim, and Seth Lloyd. “Quantum algorithm for linear systems of equations”. *Physical review letters* **103**, 150502 (2009).
- [4] Guang Hao Low and Isaac L. Chuang. “Hamiltonian simulation by qubitization”. *Quantum* **3**, 163 (2019).
- [5] John Preskill. “Quantum computing in the NISQ era and beyond”. *Quantum* **2**, 79 (2018).
- [6] Alberto Peruzzo, Jarrod McClean, Peter Shadbolt, Man-Hong Yung, Xiao-Qi Zhou, Peter J. Love, Alán Aspuru-Guzik, and Jeremy L. O’Brien. “A variational eigenvalue solver on a photonic quantum processor”. *Nature communications* **5**, 1–7 (2014).
- [7] Carlos Bravo-Prieto, Ryan LaRose, M. Cerezo, Yigit Subasi, Lukasz Cincio, and Patrick J. Coles. “Variational Quantum Linear Solver” (2020). [arXiv:1909.05820](https://arxiv.org/abs/1909.05820).
- [8] Xiao Yuan, Suguru Endo, Qi Zhao, Ying Li, and Simon C. Benjamin. “Theory of variational quantum simulation”. *Quantum* **3**, 191 (2019).
- [9] Xin Wang, Zhixin Song, and Youle Wang. “Variational quantum singular value decomposition”. *Quantum* **5**, 483 (2021).
- [10] Fan-Xu Meng, Ze-Tong Li, Xutao Yu, and Zaichen Zhang. “Quantum algorithm for MUSIC-based DOA estimation in hybrid MIMO systems”. *Quantum Science and Technology* (2021).
- [11] Ze-Tong Li, Fan-Xu Meng, Xu-Tao Yu, and Zai-Chen Zhang. “Quantum algorithm for Laplacian eigenmap via Rayleigh quotient iteration”. *Quantum Information Processing* **21**, 1–20 (2022).
- [12] Kerstin Beer, Dmytro Bondarenko, Terry Farrelly, Tobias J. Osborne, Robert Salzmann, Daniel Scheiermann, and Ramona Wolf. “Training deep quantum neural networks”. *Nature Communications* **11**, 808 (2020).
- [13] Amira Abbas, David Sutter, Christa Zoufal, Aurelien Lucchi, Alessio Figalli, and Stefan Woerner. “The power of quantum neural networks”. *Nature Computational Science* **1**, 403–409 (2021).

- [14] Jacob Biamonte, Peter Wittek, Nicola Pancotti, Patrick Rebentrost, Nathan Wiebe, and Seth Lloyd. “Quantum machine learning”. *Nature* **549**, 195–202 (2017).
- [15] Vojtěch Havlíček, Antonio D. Córcoles, Kristan Temme, Aram W. Harrow, Abhinav Kandala, Jerry M. Chow, and Jay M. Gambetta. “Supervised learning with quantum-enhanced feature spaces”. *Nature* **567**, 209–212 (2019).
- [16] Abhinav Kandala, Antonio Mezzacapo, Kristan Temme, Maika Takita, Markus Brink, Jerry M Chow, and Jay M Gambetta. “Hardware-efficient variational quantum eigensolver for small molecules and quantum magnets”. *Nature* **549**, 242–246 (2017).
- [17] Yuxuan Du, Tao Huang, Shan You, Min-Hsiu Hsieh, and Dacheng Tao. “Quantum circuit architecture search: Error mitigation and trainability enhancement for variational quantum solvers” (2020). [arXiv:2010.10217](https://arxiv.org/abs/2010.10217).
- [18] Jarrod R McClean, Sergio Boixo, Vadim N Smelyanskiy, Ryan Babbush, and Hartmut Neven. “Barren plateaus in quantum neural network training landscapes”. *Nature communications* **9**, 1–6 (2018).
- [19] Taylor L. Patti, Khadijeh Najafi, Xun Gao, and Susanne F. Yelin. “Entanglement devised barren plateau mitigation”. *Physical Review Research* **3**, 033090 (2021).
- [20] Carlos Ortiz Marrero, Mária Kieferová, and Nathan Wiebe. “Entanglement-Induced Barren Plateaus”. *PRX Quantum* **2**, 040316 (2021).
- [21] Marco Cerezo, Akira Sone, Tyler Volkoff, Lukasz Cincio, and Patrick J. Coles. “Cost function dependent barren plateaus in shallow parametrized quantum circuits”. *Nature communications* **12**, 1–12 (2021).
- [22] Stefan H. Sack, Raimel A. Medina, Alexios A. Michailidis, Richard Kueng, and Maksym Serbyn. “Avoiding barren plateaus using classical shadows” (2022). [arXiv:2201.08194](https://arxiv.org/abs/2201.08194).
- [23] Zoë Holmes, Kunal Sharma, M. Cerezo, and Patrick J. Coles. “Connecting ansatz expressibility to gradient magnitudes and barren plateaus”. *PRX Quantum* **3**, 010313 (2022). [arXiv:2101.02138](https://arxiv.org/abs/2101.02138).
- [24] Samson Wang, Enrico Fontana, Marco Cerezo, Kunal Sharma, Akira Sone, Lukasz Cincio, and Patrick J. Coles. “Noise-induced barren plateaus in variational quantum algorithms”. *Nature communications* **12**, 1–11 (2021).
- [25] Arthur G. Rattew, Shaohan Hu, Marco Pistoia, Richard Chen, and Steve Wood. “A Domain-agnostic, Noise-resistant, Hardware-efficient Evolutionary Variational Quantum Eigensolver” (2020). [arXiv:1910.09694](https://arxiv.org/abs/1910.09694).
- [26] Shi-Xin Zhang, Chang-Yu Hsieh, Shengyu Zhang, and Hong Yao. “Differentiable Quantum Architecture Search” (2021). [arXiv:2010.08561](https://arxiv.org/abs/2010.08561).
- [27] Mateusz Ostaszewski, Lea M. Trenkwalder, Wojciech Masarczyk, Eleanor Scerri, and Vedran Dunjko. “Reinforcement learning for optimization of variational quantum circuit architectures”. In *Advances in Neural Information Processing Systems*. Volume 34, pages 18182–18194. Curran Associates, Inc. (2021).
- [28] M. Bilkis, M. Cerezo, Guillaume Verdon, Patrick J. Coles, and Lukasz Cincio. “A semi-agnostic ansatz with variable structure for quantum machine learning” (2022). [arXiv:2103.06712](https://arxiv.org/abs/2103.06712).
- [29] Zi-Jian Zhang, Thi Ha Kyaw, Jakob Kottmann, Matthias Degroote, and Alan Aspuru-Guzik. “Mutual information-assisted adaptive variational quantum eigensolver”. *Quantum Science and Technology* (2021).
- [30] Fanxu Meng, Ze-Tong Li, Xu-Tao Yu, and Zai-Chen Zhang. “Quantum Circuit Architecture Optimization for Variational Quantum Eigensolver via Monte-Carlo Tree Search”. *IEEE Transactions on Quantum Engineering* (2021).

- [31] D. Chivilikhin, A. Samarin, V. Ulyantsev, I. Iorsh, A. R. Oganov, and O. Kyriienko. “MoG-VQE: Multiobjective genetic variational quantum eigensolver” (2020). [arXiv:2007.04424](#).
- [32] Thomas Elsken, Jan Hendrik Metzen, and Frank Hutter. “Neural Architecture Search: A Survey” (2019). [arXiv:1808.05377](#).
- [33] Kosuke Mitarai, Makoto Negoro, Masahiro Kitagawa, and Keisuke Fujii. “Quantum circuit learning”. *Physical Review A* **98**, 032309 (2018).
- [34] Philip Wolfe. “Convergence conditions for ascent methods”. *SIAM review* **11**, 226–235 (1969).
- [35] Sukin Sim, Peter D. Johnson, and Alán Aspuru-Guzik. “Expressibility and entangling capability of parameterized quantum circuits for hybrid quantum-classical algorithms”. *Advanced Quantum Technologies* **2**, 1900070 (2019).
- [36] Kouhei Nakaji and Naoki Yamamoto. “Expressibility of the alternating layered ansatz for quantum computation”. *Quantum* **5**, 434 (2021).
- [37] Marco Cerezo and Patrick J. Coles. “Higher order derivatives of quantum neural networks with barren plateaus”. *Quantum Science and Technology* **6**, 035006 (2021).
- [38] Andrew Arrasmith, M. Cerezo, Piotr Czarnik, Lukasz Cincio, and Patrick J. Coles. “Effect of barren plateaus on gradient-free optimization”. *Quantum* **5**, 558 (2021).
- [39] Daniel Stilck França and Raul Garcia-Patron. “Limitations of optimization algorithms on noisy quantum devices”. *Nature Physics* **17**, 1221–1227 (2021).
- [40] Arthur Pesah, M. Cerezo, Samson Wang, Tyler Volkoff, Andrew T. Sornborger, and Patrick J. Coles. “Absence of barren plateaus in quantum convolutional neural networks”. *Physical Review X* **11**, 041011 (2021).
- [41] Tyler Volkoff and Patrick J. Coles. “Large gradients via correlation in random parameterized quantum circuits”. *Quantum Science and Technology* **6**, 025008 (2021).
- [42] Andrea Skolik, Jarrod R. McClean, Masoud Mohseni, Patrick van der Smagt, and Martin Leib. “Layerwise learning for quantum neural networks”. *Quantum Machine Intelligence* **3**, 1–11 (2021).
- [43] Edward Grant, Leonard Wossnig, Mateusz Ostaszewski, and Marcello Benedetti. “An initialization strategy for addressing barren plateaus in parametrized quantum circuits”. *Quantum* **3**, 214 (2019).
- [44] Guillaume Verdon, Michael Broughton, Jarrod R. McClean, Kevin J. Sung, Ryan Babbush, Zhang Jiang, Hartmut Neven, and Masoud Mohseni. “Learning to learn with quantum neural networks via classical neural networks” (2019). [arXiv:1907.05415](#).
- [45] Shan You, Tao Huang, Mingmin Yang, Fei Wang, Chen Qian, and Changshui Zhang. “GreedyNAS: Towards fast one-shot NAS with greedy supernet”. In Proceedings of the IEEE/CVF Conference on Computer Vision and Pattern Recognition. *Pages 1999–2008*. IEEE (2020).
- [46] Alba Cervera-Lierta, Jakob S. Kottmann, and Alán Aspuru-Guzik. “Meta-variational quantum eigensolver: Learning energy profiles of parameterized hamiltonians for quantum simulation”. *PRX Quantum* **2**, 020329 (2021).
- [47] Ville Bergholm, Josh Izaac, Maria Schuld, Christian Gogolin, M. Sohaib Alam, Shahnawaz Ahmed, Juan Miguel Arrazola, Carsten Blank, Alain Delgado, Soran Jahangiri, Keri McKiernan, Johannes Jakob Meyer, Zeyue Niu, Antal Száva, and Nathan Killoran. “PennyLane: Automatic differentiation of hybrid quantum-classical computations” (2020). [arXiv:1811.04968](#).

A Examples

Example 1 (A VQE Task). *The VQE is to find the ground state energy of a quantum system where the dynamic can be described by a Hamiltonian H . Setting the observable $O = H$, the function $f(x) = x$, the input state $\rho = |0\rangle\langle 0|$, and the ansatz $U(\boldsymbol{\theta})$ as the hardware efficient ansatz (c.f. Appendix B), where $\boldsymbol{\theta} \in (-\pi, \pi]^d$ and d is the number of parameters, the problem is*

$$\min_{\boldsymbol{\theta} \in (-\pi, \pi]^d} C(\boldsymbol{\theta}) = \text{Tr} \left[H U(\boldsymbol{\theta}) |0\rangle\langle 0| U^\dagger(\boldsymbol{\theta}) \right]. \quad (37)$$

Example 2 (Not Bijection). *For a 2-qubit quantum system, $N_l = 2$, define \mathbf{s}_1 and \mathbf{s}_2 as $(I^{q_1}, R_y^{q_2})$ and $(R_z^{q_1}, I^{q_2})$, respectively. Then, the practical implementations of two ansatzes described by paths*

$$\begin{aligned} \mathbf{p}_1 &= (\mathbf{v}^0, \mathbf{v}_1^1 := (\mathbf{v}^0, \mathbf{s}_1), \mathbf{v}_1^2 := (\mathbf{v}^1, \mathbf{s}_2)), \\ \mathbf{p}_2 &= (\mathbf{v}^0, \mathbf{v}_2^1 := (\mathbf{v}^0, \mathbf{s}_2), \mathbf{v}_2^2 := (\mathbf{v}^1, \mathbf{s}_1)) \end{aligned}$$

are identical.

Example 3 (Mergeable & Deletable). *For a 4-qubit quantum system, $N_l = 2$, define*

$$\begin{aligned} \mathbf{s}_1 &:= (I^{q_1}, R_y^{q_2}, \text{CNOT}^{q_3, q_4}), \\ \mathbf{s}_2 &:= (R_z^{q_1}, R_y^{q_2}, \text{CNOT}^{q_3, q_4}), \\ \mathbf{s}_3 &:= (R_z^{q_1}, R_y^{q_2}). \end{aligned}$$

Then, the practical implementations of two ansatzes described by paths

$$\begin{aligned} \mathbf{p}_1 &= (\mathbf{v}^0, \mathbf{v}_1^1 := (\mathbf{v}^0, \mathbf{s}_1), \mathbf{v}_1^2 := (\mathbf{v}^1, \mathbf{s}_2)), \\ \mathbf{p}_2 &= (\mathbf{v}^0, \mathbf{v}_2^1 := (\mathbf{v}^0, \mathbf{s}_3), \mathbf{v}_2^2 := (\mathbf{v}^1, ())) \end{aligned}$$

are equivalent.

Example 4 (Size of Search Space). *The number of possible paths in a 4-qubit quantum system under the setting as described in Sec. 2.6 with and without the gates commutation rules $N_{w/}$ and $N_{w/o}$ with respect to N_l are demonstrated in Tab.3*

Table 3: The number of possible paths with respect to N_l .

| N_l | $N_{w/}$ | $N_{w/o}$ | $\frac{N_{w/}}{N_{w/o}}$ |
|-------|----------|-----------|--------------------------|
| 1 | 56 | 567 | 9.88% |
| 2 | 11768 | 321489 | 3.66% |
| 3 | 2859977 | 182284263 | 1.57% |

B Hardware efficient ansatz

The hardware efficient ansatz (HEA) was first proposed in [16] to conduct VQE for small molecules and quantum magnets. It is constructed in a layer-by-layer fashion in which each layer has an identical structure. Specifically, a layer is organized by native single-qubit gates on all qubits and naturally available entangling interactions. In our setting, based on the native gates as described in Sec. 2.6, we exploit the HEA with layers as depicted in Fig. 10.

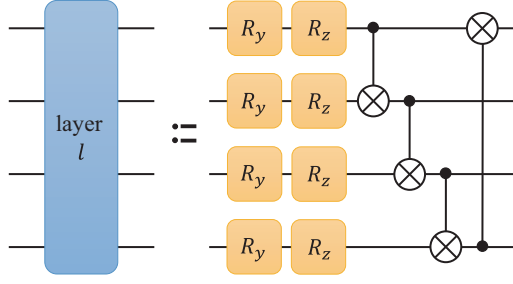


Figure 10: Layer construction used in HEA.

C Proof of Theorem 1

Solution of Prob. 1 is a set of parameters

$$\Theta^* = \{\boldsymbol{\theta}^* | C(\boldsymbol{\theta}^*) = \min_{\boldsymbol{\theta} \in \mathbb{D}^d} C(\boldsymbol{\theta})\}. \quad (38)$$

$$\left\{ (U^*, \Theta^*) \left| \begin{array}{l} C(U^*, \boldsymbol{\theta}^*) = \min_{U, \boldsymbol{\theta}} C(U, \boldsymbol{\theta}), \\ \forall \boldsymbol{\theta}^* \in \Theta^* \end{array} \right. \right\}. \quad (39)$$

Given an arbitrary valid \mathbb{P} , we divide \mathbb{S} into four disjoint sets

$$\mathbb{U}_+^* \equiv \left\{ U \left| C(U, \boldsymbol{\theta}_U) = \min_{U, \boldsymbol{\theta}} C(U, \boldsymbol{\theta}) \right. \right\}, \quad (40)$$

$$\mathbb{U}_+ \equiv \left\{ U \left| \exists \boldsymbol{\theta}', C(U, \boldsymbol{\theta}') = \min_{U, \boldsymbol{\theta}} C(U, \boldsymbol{\theta}), C(U, \boldsymbol{\theta}_U) > \min_{\boldsymbol{\theta}} C(U, \boldsymbol{\theta}) \right. \right\}, \quad (41)$$

$$\mathbb{U}_-^* \equiv \left\{ U \left| \forall \boldsymbol{\theta}', C(U, \boldsymbol{\theta}') > \min_{U, \boldsymbol{\theta}} C(U, \boldsymbol{\theta}), C(U, \boldsymbol{\theta}_U) = \min_{\boldsymbol{\theta}} C(U, \boldsymbol{\theta}) \right. \right\}, \quad (42)$$

$$\mathbb{U}_- \equiv \left\{ U \left| \forall \boldsymbol{\theta}', C(U, \boldsymbol{\theta}') > \min_{U, \boldsymbol{\theta}} C(U, \boldsymbol{\theta}), C(U, \boldsymbol{\theta}_U) > \min_{\boldsymbol{\theta}} C(U, \boldsymbol{\theta}) \right. \right\}. \quad (43)$$

Note that $\mathbb{U}_+^* \cup \mathbb{U}_+ \cup \mathbb{U}_-^* \cup \mathbb{U}_- = \mathbb{S}$. We prove the theorem by proving

$$\lim_{t \rightarrow \infty} \mathbb{U}_n \cap (\mathbb{U}_-^* \cup \mathbb{U}_-) = \emptyset, \quad (44)$$

$$\lim_{t \rightarrow \infty} \mathbb{U}_n = \lim_{t \rightarrow \infty} \mathbb{U}_+^*, \quad (45)$$

where t indicates the iteration of the alternate optimization loop.

Lemma 1. $U \in \lim_{t \rightarrow \infty} \mathbb{U}_+^* \cup \mathbb{U}_-^*, \forall U \in \mathbb{U}_+ \cup \mathbb{U}_-$ such that $\frac{\|\nabla C(U, \boldsymbol{\theta}_U)\|_2}{|\boldsymbol{\theta}_U|} > 0$.

Proof. By solving the Prob. 3, all ansatzes $U \in \mathbb{U}_+ \cup \mathbb{U}_-$ such that

$$\frac{\|\nabla C(U, \boldsymbol{\theta}_U)\|_2}{|\boldsymbol{\theta}_U|} = \max_{\boldsymbol{\theta}} \frac{\|\nabla C(U, \boldsymbol{\theta})\|_2}{|\boldsymbol{\theta}|} > 0$$

are included in \mathbb{U}_n . For any $U \in \mathbb{U}_n$, $\boldsymbol{\theta}_U \in \mathbb{P}$ is updated by $\boldsymbol{\theta}^*$ such that $C(U, \boldsymbol{\theta}^*) = \min_{\boldsymbol{\theta}} C(U, \boldsymbol{\theta})$, which means any $U \in \mathbb{U}_n$ is an element of $U \in \mathbb{U}_+^* \cup \mathbb{U}_-^*$ in the next iteration. Therefore, any $U \in \mathbb{U}_+ \cup \mathbb{U}_-$ such that $\frac{\|\nabla C(U, \boldsymbol{\theta}_U)\|_2}{|\boldsymbol{\theta}_U|} > 0$ will be selected as an element in \mathbb{U}_n if $t \rightarrow \infty$. Then, we have $U \in \lim_{t \rightarrow \infty} \mathbb{U}_+^* \cup \mathbb{U}_-^*, \forall U \in \mathbb{U}_+ \cup \mathbb{U}_-$ such that $\frac{\|\nabla C(U, \boldsymbol{\theta}_U)\|_2}{|\boldsymbol{\theta}_U|} > 0$. \square

Further, it is straightforward that $U \in \lim_{t \rightarrow \infty} \mathbb{U}_+^*$, $\forall U \in \mathbb{U}_+$ such that $\frac{\|\nabla C(U, \theta_U)\|_2}{|\theta_U|} > 0$ and $V \in \lim_{t \rightarrow \infty} \mathbb{U}_-^*$, $\forall V \in \mathbb{U}_-$ such that $\frac{\|\nabla C(V, \theta_V)\|_2}{|\theta_V|} > 0$. Since $C(U, \theta_U) = \min_{\theta} C(U, \theta)$ for all $U \in \mathbb{U}_+^* \cup \mathbb{U}_-^*$, we have that

$$\frac{\|\nabla C(U, \theta_U)\|_2}{|\theta_U|} = 0, \quad \forall U \in \mathbb{U}_+^* \cup \mathbb{U}_-^*. \quad (46)$$

Therefore, if \mathbb{U}_+^* is not empty, then inequalities Eq. (23) and Eq. (24) are simultaneously established for all $U \in \mathbb{U}_-^*$, $V \in \mathbb{U}_+^*$, which means $\mathbb{U}_n \cap \mathbb{U}_-^* = \emptyset$. Then, we have that

$$\lim_{t \rightarrow \infty} \mathbb{U}_n \cap (\mathbb{U}_-^* \cup \mathbb{U}_+) = \emptyset, \quad (47)$$

if $\lim_{t \rightarrow \infty} \mathbb{U}_+^* \neq \emptyset$.

The simultaneous establishment of Eq. (25) and Eq. (26) of V implies that $V \in \mathbb{U}_+$ with $\frac{\|\nabla C(V, \theta_V)\|_2}{|\theta_V|} > 0$ or $V \in \mathbb{U}_+^*$, which indicates

$$\lim_{t \rightarrow \infty} \mathbb{U}_+^* \neq \emptyset. \quad (48)$$

It is obvious that $\mathbb{U}_+^* \subset \mathbb{U}_n$ and $\mathbb{U}_n \subset \mathbb{U}_+^* \cup \mathbb{U}_+$. Since

$$\lim_{t \rightarrow \infty} \mathbb{U}_+ \equiv \left\{ U \left| \begin{array}{l} \exists \theta', C(U, \theta') = \min_{U, \theta} C(U, \theta), \\ \forall \delta > 0, C(U, \theta_U \in \lim_{t \rightarrow \infty} \mathbb{P}) = \max_{\theta \in \Theta_{U, \delta}} C(U, \theta) \end{array} \right. \right\}, \quad (49)$$

where $\Theta_{U, \delta} = \{\theta \mid \|\theta - \theta_U\|_2 < \delta\}$, we have that $\lim_{t \rightarrow \infty} (\mathbb{U}_n \cup \mathbb{U}_+) = \emptyset$. Therefore, Eq. (44) and Eq. (45) are established.

D Hyperparameters

Table 4: Hyperparameters.

| scope | name | notation |
|--------------------|--|--------------------------|
| global | maximum number of layers | N_l |
| | reference step size | α_0 |
| | convergence threshold | ξ |
| | probabilities for double ϵ -greedy strategy | ϵ_1, ϵ_2 |
| pool training | number of sampled ansatzes | N_{s1} |
| | maximum number of ranks for updating parameters | N_{r1} |
| | stable threshold for terminating | N_{t1} |
| | maximum iteration times in the prethermalization | N_{i0} |
| | maximum iteration times in the main process | N_{i1} |
| alternate training | population size | N_{s2} |
| | maximum number of ranks for updating parameters | N_{r2} |
| | stable threshold for terminating | N_{t2} |
| | optimization step per generation | N_o |
| VQE retraining | maximum iteration times | N_{i2} |
| | maximum iteration times | N_{i3} |

E Genetic Operators

In this appendix, we provide genetic operators the GSA applied in detail. We only consider the asexual genetic operators for simplicity. Consequently, only one ansatz is generated from each survival ansatz. All genetic operators comply with the same structure. First, a new practical implementation of ansatz is randomly generated. Then, the implementation is refined by the gate commutation rule. Since the bijection between the search space and the practical implementations of ansatzes is established, the path representation of the new implementation is finally output. We introduce the genetic operators identified in the first step.

Mutation: The mutation operator randomly selects a node \mathbf{v} in the survival ansatz. Then, a child node \mathbf{v}_{new} of the parent node of \mathbf{v} is randomly sampled. Therefore, a new implementation of ansatz substituting \mathbf{v} by \mathbf{v}_{new} is generated.

Deletion: The deletion operator randomly deletes a node in the survival ansatz and connects its parent node and child node. Then, a new implementation is generated.

Amplification: The amplification operator randomly selects a node \mathbf{v} in the survival ansatz. Then, a child node of \mathbf{v} is inserted into the ansatz, and therefore a new implementation is generated.

F Pseudocodes for Algorithms

In this appendix, we list the pseudocodes for algorithms. Note that the task \mathbb{T} is generally omitted as the input parameters of algorithms without confusion.

Algorithm 1: alternate VA-VQE

```
Input:  $\mathbb{S}, \mathbb{P}_0$   
begin  
   $\mathbb{P} \leftarrow \mathbb{P}_0;$  // Initialize  $\mathbb{P}$   
   $\mathbb{U}_n \leftarrow \{\};$  // Initialize  $\mathbb{U}_n$   
  while  $\mathbb{U}_n$  and  $\mathbb{P}$  are not converged do  
     $\mathbb{U}_n \leftarrow \mathbf{SolveProb3}(\mathbb{S}, \mathbb{P});$   
    foreach  $U \in \mathbb{U}_n$  do  
       $\theta_U \in \mathbb{P} \leftarrow \mathbf{SolveProb1}(U);$   
    end  
  end  
end  
return  $\mathbb{U}_n, \mathbb{P}.$ 
```

Algorithm 2: GSA

Input: \mathbb{G}
begin
 $\mathbb{S}(N_l) \leftarrow$ Construct search space by \mathbb{G} ;
 $\mathbb{P}_0, T \leftarrow \mathbf{PoolTraining}(\mathbb{S}(N_l))$;
 $U^*, \theta_{U^*} \leftarrow \mathbf{AlternateTraining}(\mathbb{S}(N_l), \mathbb{P}_0, T)$;
 $U^*, \theta^* \leftarrow \mathbf{VQETraining}(U^*, \theta_{U^*})$;
end
return U^*, θ^* .

Algorithm 3: USampling

Input: $\mathbb{S}(N_l), T, \epsilon_1, \epsilon_2$
begin
 $J_1 \sim \{(True, \epsilon_1), (False, 1 - \epsilon_1)\}$;
 if J_1 *is True* **then**
 $\mathbf{v} \leftarrow \mathbf{v}^0 \in T$;
 $U \leftarrow (\mathbf{v})$;
 $\eta \sim \{(1, \epsilon_2), (0, 1 - \epsilon_2)\}$;
 for \mathbf{v} *is not a leaf node* **do**
 $\mathbb{V}_c \leftarrow \mathbf{GetChildNodes}(\mathbf{v})$;
 $\mathbf{v}' \sim \{(\mathbf{v}'_k \in \mathbb{V}_c, \text{Pr}(\mathbf{v}'_k; \eta))\}$;
 $U \leftarrow U \oplus (\mathbf{v}')$;
 $\mathbf{v} \leftarrow \mathbf{v}'$;
 end
 else
 $U \sim \mathbb{S}(N_l)$;
 end
end
return U .

Algorithm 4: PoolTrainingMainProcess

Input: $\mathbb{S}(N_l)$, P , T **begin** $\mathbb{S} \leftarrow \mathbb{S}(N_l)$; $t \leftarrow 0$; $c'_l \leftarrow 1$; $i \leftarrow 1$; **for** $i \leq N_{i1}$ **do** $\mathbb{U}_s \leftarrow \{\}$; **for** $|\mathbb{U}_s| < N_{s1}$ **do** $U \leftarrow \text{USampling}(\mathbb{S}, T, \epsilon_1, \epsilon_2)$; $\mathbb{U}_s \leftarrow \mathbb{U}_s \cup \{U\}$; **end** $\mathbb{U}_n(N_{r1}) \leftarrow \text{SolveProb3}(\mathbb{U}_s, P)$; **foreach** $U \in \mathbb{U}_n(N_{r1})$ **do** $\theta \leftarrow \text{GetParameters}(U, P)$; $\alpha \leftarrow \text{GetStepSize}(\alpha_0)$; $\theta \leftarrow \theta - \alpha \nabla C(U, \theta)$; $P \leftarrow \text{UpdatePool}(\theta, P)$; $T \leftarrow \text{Append } U \text{ on the candidate tree } T$; **end** **if** $c_l(\mathbf{v}^0) = c'_l$ **then** $t \leftarrow t + 1$; **if** $t = N_{t1}$ **then** **break**; **end** **else** $t \leftarrow 0$; $c'_l \leftarrow c_l(\mathbf{v}^0)$; **end** $i \leftarrow i + 1$; **end****end****return** P , T .

Algorithm 5: PoolTrainingPrethermalization

Input: $\mathbb{S}(N_l)$, P , T

begin

- $\mathbb{S} \leftarrow \mathbb{S}(N_l)$;
- $i \leftarrow 1$
- $\epsilon'_1 = (i - 1)\epsilon_1/N_{i0}$;
- for** $i \leq N_{i1}$ **do**
 - $\mathbb{U}_s \leftarrow \{\}$;
 - for** $|\mathbb{U}_s| < N_{s1}$ **do**
 - $U \leftarrow \mathbf{USampling}(\mathbb{S}, T, \epsilon'_1, \epsilon_2)$;
 - $\mathbb{U}_s \leftarrow \mathbb{U}_s \cup \{U\}$;
 - $j \leftarrow j + 1$;
 - end**
 - $\mathbb{U}_n(N_{r1}) \leftarrow \mathbf{SolveProb3}(\mathbb{U}_s, P)$;
 - foreach** $U \in \mathbb{U}_n(N_{r1})$ **do**
 - $\theta \leftarrow \mathbf{GetParameters}(U, P)$;
 - $\alpha \leftarrow \mathbf{GetStepSize}(\alpha_0)$;
 - $\theta \leftarrow \theta - \alpha \nabla C(U, \theta)$;
 - $P \leftarrow \mathbf{UpdatePool}(\theta, P)$;
 - $T \leftarrow \mathbf{Append } U \text{ on the candidate tree } T$;
 - end**
 - $i \leftarrow i + 1$;
- end**
- $\mathbb{P}_0 \leftarrow \mathbf{Expand}(P)$;

end

return P , T .

Algorithm 6: PoolTraining

Input: $\mathbb{S}(N_l)$

begin

- $P \leftarrow$ Construct parameter pool with $\mathbf{0}$ initialization;
- $T \leftarrow \{\mathbf{v}^0\}$;
- $P, T \leftarrow \mathbf{PoolTrainingPrethermalization}(\mathbb{S}(N_l), P, T)$;
- $P, T \leftarrow \mathbf{PoolTrainingMainProcess}(\mathbb{S}(N_l), P, T)$;
- $\mathbb{P}_0 \leftarrow \mathbf{Expand}(P)$;

end

return \mathbb{P}_0 , T .

Algorithm 7: AlternateTraining

Input: $\mathbb{S}(N_l), \mathbb{P}_0, T$ **begin** $\mathbb{P} \leftarrow \mathbb{P}_0$ $\mathbb{U}_s \leftarrow \{\};$ $U_{best} \leftarrow \mathbf{None};$ **for** $|\mathbb{U}_s| \leq N_{s2}$ **do** $U \leftarrow \mathbf{USampling}(\mathbb{S}, T, \epsilon_1, \epsilon_2);$ $\mathbb{U}_s \leftarrow \mathbb{U}_s \cup \{U\};$ **end** $i \leftarrow 1;$ **for** $i \leq N_{i2}$ **do** $\mathbb{U}_n(N_{r2}), \mathbb{U}_n(N'_r), \mathbb{U}_n(N'_r + 1) \leftarrow \mathbf{SolveProb3}(\mathbb{U}_s, \mathbb{P});$ **foreach** $U \in \mathbb{U}_n(N_{r2})$ **do** $j \leftarrow 1;$ **for** $j \leq N_o$ **do** $\alpha \leftarrow \mathbf{GetStepSize}(\alpha_0);$ $\theta_U \leftarrow \theta_U - \alpha \nabla C(U, \theta_U);$ $j \leftarrow j + 1;$ **end****end** $\mathbb{U}_{survival} \leftarrow \mathbf{GetSurvivals}(\mathbb{U}_n(N'_r), \mathbb{U}_n(N'_r + 1));$ **if** $\exists U \in \mathbb{U}_{survival}$ such that $C(U, \theta_U) < C(U_{best}, \theta_{U_{best}})$ **then** $U_{best} \leftarrow \mathbf{None};$ **end** $\mathbb{U}_{new} \leftarrow \{\};$ **foreach** $U \in \mathbb{U}_{survival}$ **do** $U_{new} \leftarrow \mathbf{RandomGeneticOperator}(U);$ $\mathbb{U}_{new} \leftarrow \mathbb{U}_{new} \cup \{U_{new}\};$ $\alpha \leftarrow \mathbf{GetStepSize}(\alpha_0);$ **if** $\alpha \frac{\|\nabla C(U, \theta_U)\|_2}{|\theta_U|} < \xi$ **then** $\mathbb{U}_{survival} \leftarrow \mathbb{U}_{survival} \setminus \{U\};$ **if** $C(U, \theta_U) < C(U_{best}, \theta_{U_{best}})$ **then** $U_{best} \leftarrow U;$ **end****end****end** $\mathbb{U}_s \leftarrow \mathbb{U}_{survival} \cap \mathbb{U}_{new};$ **for** $|\mathbb{U}_s| \leq N_{s2}$ **do** $U \leftarrow \mathbf{USampling}(\mathbb{S}, T, \epsilon_1, \epsilon_2);$ $\mathbb{U}_s \leftarrow \mathbb{U}_s \cup \{U\};$ **end****if** U_{best} has been preserved for N_{i2} generations **then** $\mathbf{break};$ **end****end** $U^* \leftarrow \arg \min_{U \in \mathbb{U}_s \cup \{U_{best}\}} C(U, \theta_U);$ **end****return** $U^*, \theta_{U^*}.$

Algorithm 8: VQERetraining

Input: U, θ_0

begin

$\theta \leftarrow \theta_0;$

$i \leftarrow 1$

for $i \leq N_{i3}$ **do**

$\alpha \leftarrow \text{GetStepSize}(\alpha_0);$

$\theta \leftarrow \theta - \alpha \nabla C(U, \theta);$

$i \leftarrow i + 1;$

if $\alpha \frac{\|\nabla C(U, \theta)\|_2}{|\theta|} < \xi$ **then**

break;

end

end

$U^* \leftarrow U, \theta^* \leftarrow \theta;$

end

return $U^*, \theta^*.$
